JOURNAL OF SOLID STATE CHEMISTRY **127,** 248–255 (1996)
ARTICLE NO. 0381

New Anion-Excess, Fluorite-Related, Ordered Structure: $Bi_2Te_2W_3O_{16}$

J. C. Champarnaud-Mesjard and B. Frit[1]

Laboratoire de Matériaux Céramiques et Traitements de Surface, URA CNRS No. 320, 123, Avenue Albert-Thomas, 87060 Limoges Cedex, France

and

A. Chagraoui and A. Tairi

Département de Chimie, Faculté des Sciences Ben M'Sik, Université Hassan II-Mohammédia, Casablanca, Morocco

Received June 18, 1996; in revised form September 10, 1996; accepted September 12, 1996

A solid-state investigation of the Bi_2O_3–TeO_2–WO_3 system allowed synthesis of a new stoichiometric compound, $Bi_2Te_2W_3O_{16}$ ($MX_{2.286}$). $Bi_2Te_2W_3O_{16}$ crystallizes with monoclinic symmetry (space group $C2/c$) with the unit cell parameters a = 21.2871(8) Å, b = 5.5708(3), c = 12.8349(5) Å, β = 124.08(3)°, and Z = 4 formula units per cell. The structure was determined from single-crystal X-ray diffraction data and refined to residuals $R_1(F) = 0.036$ and $wR_2(F^2) = 0.089$ for 106 variable parameters and a data set of 1756 observations [$I > 2\sigma(I)$]. The essential building units of the structure are BiO_8 square antiprisms, TeO_4 disphenoids, and WO_6 octahedra. Pairs of BiO_8 square antiprisms share one edge to form a Bi_2O_{14} unit. Each Bi_2O_{14} unit shares four corners with four identical Bi_2O_{14} units, two edges and four corners with $W(2)O_6$ octahedra, and four edges with TeO_4 disphenoids, so constituting [$Bi_2Te_2W(2)_2O_{16}$] complex layers parallel to (100). These layers are connected via $W(1)O_6$ to form the $Bi_2Te_2W_3O_{16}$ three-dimensional network. Its relationships with the fluorite structure and the fluorite-related $Bi_7O_5F_{11}$ structure are evidenced and analyzed. © 1996 Academic Press

INTRODUCTION

TeO_2-based systems, including oxides of heavy elements like bismuth (III) and tungsten (VI), are of interest in the formation of glasses with nonlinear optical properties. The reinvestigation of the pseudoternary Bi_2O_3–TeO_2–WO_3 system (1), which is promising as a basis in the creation of such glasses, showed, in addition to a large glass formation region, the existence of several strictly stoichiometric, anion-excess or anion-deficient ordered fluorite-related phases. Such phases are interesting since they often exhibit original physical properties related to the crystallochemical behavior of Bi(III) and Te(IV) atoms. This paper describes the crystal structure of one of these new phases, $Bi_2Te_2W_3O_{16}$, and its relationships with the fluorite and $Bi_7O_5F_{11}$ structures.

EXPERIMENTAL

Heating in air at 720°C for 48 h an intimate mixture of pure commercial Bi_2O_3, TeO_2, and WO_3 oxides (Aldrich, 99.99%) in the molar ratio 1:2:3 led to the formation, in the solid state and as a green polycrystalline powder, of an original solid phase with the probable formula $Bi_2Te_2W_3O_{16}$. Since no significant change in weight was observed, and since the same solid phase was obtained when the synthesis was performed in a sealed gold tube, it was clear that no oxidation of Te(IV) had occurred and that the formula proposed was correct.

$Bi_2Te_2W_3O_{16}$ is stable only below 750°C; above this temperature it decomposes into two crystalline phases, WO_3 and $Bi_2W_2O_9$, and a liquid phase, which on cooling leads to the formation of a ternary glass of unidentified composition.

Its X-ray powder pattern (Table 1) recorded with a Siemens D-5000 diffractometer has been indexed using the ITO program (2) on the basis of a centered monoclinic cell with the following parameters: a = 21.2871(8) Å, b = 5.5708(3) Å, c = 12.8349(5) Å, β = 124.03(3)°.

Good single crystals were obtained together with a glassy phase by melting at 760°C, slowly cooling (1°C/h) to 700°C, and then air quenching a mixture of the three oxides richer in TeO_2 (Bi_2O_3:TeO_2:WO_3 = 1:4:3). One of them with the dimensions 0.10 × 0.08 × 0.16 mm^3, apparently untwinned under polarized light, was selected and mounted on a Siemens P4 four-circle automatic diffractomer. The diffraction data were registered under the conditions given

[1] To whom correspondence should be addressed.

0022-4596/96 $18.00
Copyright © 1996 by Academic Press
All rights of reproduction in any form reserved.

TABLE 1
X-Ray Powder Diffraction Data for $Bi_2Te_2W_3O_{16}$

hkl	d_{obs}	d_{calc}	I/I_0	*hkl*	d_{obs}	d_{calc}	I/I_0
200	8.85	8.82	4	$62\bar{4}$	2.031	2.030	7
$20\bar{2}$	6.43	6.41	8	620	2.022	2.022	4
002	5.33	5.33	3	$51\bar{6}$	1.994	1.993	6
$11\bar{1}$	5.12	5.11	1	$22\bar{3}$	1.973	1.971	3
$40\bar{2}$	5.07	5.06	4	$20\bar{6}$	1.964	1.962	7
111	4.47	4.46	2	422	1.950	1.948	2
400	4.42	4.41	2	$62\bar{5}$	1.8698	1.8681	2
$31\bar{1}$	4.39	4.38	5	$40\bar{4}$	1.8611	1.8611	16
$31\bar{2}$	4.052	4.059	22	$82\bar{1}$	1.8405	1.8387	2
$60\bar{2}$	3.554	3.548	5	$22\bar{5}$	1.8161	1.8161	3
112	3.481	3.475	39	$111\bar{5}$	1.7860	1.7851	10
311	3.378	3.372	12	$33\bar{2}$	1.7720	1.7720	2
$51\bar{1}$	3.310	3.304	100	$71\bar{7}$	1.7400	1.7396	8
$11\bar{3}$	3.213	3.209	89	802	1.7238	1.7227	4
$60\bar{4}$	2.966	2.963	42	132	1.7152	1.7135	11
020	2.789	2.785	10	$111\bar{6}$	1.7020	1.7016	3
$31\bar{4}$	2.765	2.763	4	$91\bar{7}$	1.6911	1.6910	14
312	2.745	2.748	7	$13\bar{3}$	1.6796	1.6785	4
$51\bar{4}$	2.729	2.725	21	$82\bar{6}$	1.6534	1.6522	3
$22\bar{1}$	2.689	2.686	25	530	1.6426	1.6430	1
$71\bar{2}$	2.661	2.658	10	$31\bar{5}$	1.6389	1.6393	5
511	2.574	2.570	3	$22\bar{6}$	1.6050	1.6042	2
$22\bar{3}$	2.325	2.321	1	$111\bar{7}$	1.5929	1.5920	4
$42\bar{3}$	2.307	2.305	10	$73\bar{2}$	1.5836	1.5825	6
$31\bar{5}$	2.280	2.278	3	$100\bar{8}$	1.5625	1.5624	2
$71\bar{5}$	2.227	2.226	5	$71\bar{8}$	1.5418	1.5406	2
800	2.207	2.204	3	$40\bar{8}$	1.5317	1.5313	2
$62\bar{2}$	2.192	2.191	1	$131\bar{6}$	1.5287	1.5285	1
$91\bar{3}$	2.169	2.177	2	$140\bar{6}$	1.4960	1.4960	2
$62\bar{3}$	2.146	2.148	2	$120\bar{8}$	1.4820	1.4816	5
$60\bar{6}$	2.138	2.136	3	$131\bar{7}$	1.4660	1.4659	3
$91\bar{4}$	2.132	2.136	1	$93\bar{4}$	1.4480	1.4480	1
602	2.121	2.118	1	$93\bar{1}$	1.4056	1.4063	1
$42\bar{4}$	2.103	2.102	3	$53\bar{6}$	1.4011	1.4008	6
$80\bar{6}$	2.054	2.052	10				

in Table 2 and corrected for absorption effects by using a psi-scan method [XEMP program (3)]. Three representative standard reflections measured every 100 reflections during the course of the data collection showed no significant variation in intensity.

The monoclinic symmetry and unit cell parameters derived from the powder pattern were confirmed. The observed reflection conditions are consistent with the space groups *Cc* (No. 9) and *C*2/*c* (No. 15). The experimental density [ρ_{exp} = 7.80(3) g cm^{-3}] measured by helium picnometry (Micromeritics Accupyc 1330) implies $Z = 4$ $Bi_2Te_2W_3O_{16}$ per unit cell (ρ_{th} = 7.80 g cm^{-3}).

Intensity statistics favor the centrosymmetric space group; so the structure was solved in the *C*2/*c* space group, by using direct methods and the SHELXTL-PC program package (3). In fact, all the cationic positions were determined by these methods and the oxygen atoms located by difference Fourier syntheses. By using the full-matrix least-squares techniques of the SHELXL-93 program (4) and including anisotropic thermal motion for all atoms, the structure was refined to final *R* values of $R_1(F) = 0.036$ and $wR_2(F^2) = 0.089$. Positional and thermal parameters are reported in Table 3. Selected bond lengths and angles as well as bond valences, calculated using the Brown's method (5), are given in Tables 4 and 5.

DESCRIPTION OF THE STRUCTURE

A projection onto (010) of the unit cell content is shown in Fig. 1.

Each tungsten atom is surrounded by six oxygen atoms with a mean distance ⟨W–O⟩ = 1.94 Å, in good accordance with the sum of ionic radii as proposed by Shannon (6) ($r_{W^{6+}[6]} + r_{O^{2-}[3]}$ = 1.96 Å or $r_{W^{6+}[6]} + r_{O^{2-}[2]}$ = 1.95 Å). The corresponding polyhedra are octahedra, slightly distorted in the case of W(1) atoms (Fig. 2a), strongly distorted in the case of W(2) atoms (Fig. 2b). In each case the central tungsten atom is set off-center toward the middle of an oxygen edge [O(1)–O(1) edge for W(1), O(4)–O(7) edge for W(2)]. Such eccentricity, more or less important [0.32 Å

TABLE 2
Crystal Data and Structure Refinement Conditions for $Bi_2Te_2W_3O_{16}$

Formula weight	1480.71
Temperature	293(2) K
Wavelength	0.71073 Å
Crystal system	Monoclinic
Space group	*C*2/*c*
Unit cell dimensions	
a	21.2871(8) Å
b	5.5708(3) Å
c	12.8349(5) Å
β	124.08(3)°
Volume	1260.6(1) Å^3
Z	4
Density (calculated)	7.80 Mg/m^3
Density (measured)	7.80(3) Mg/m^3
Absorption coefficient	59.728 mm^{-1}
F(000)	2480
Crystal size	0.10 × 0.08 × 0.16 mm^3
θ range for data collection	2.31 to 30.07 deg.
Index ranges	$-29 \le h \le 29$, $-1 \le k \le 7$, $-18 \le l \le 15$
Reflections collected	3959
Independent reflections	1756 [*R*(int) = 0.0553]
Refinement method	Full-matrix least-squares on F^2
Data/restraints/parameters	1756/0/106
Final *R* indices [$I > 2\sigma(I)$][a]	R_1 = 0.0365, wR_2 = 0.0894
R indices (all data)[a]	R_1 = 0.0420, wR_2 = 0.0921
Goodness-of-fit on F^2[b]	1.084
Extinction coefficient	0.00257(10)
Largest diff. peak and hole	5.758 and −4.328 *e* Å^{-3}

[a] $R_1(F) = \Sigma \; \|F_0| - |F_c\|/|F_0|$; $wR_2(F^2) = \{\Sigma \; [w(F_0^2 - F_c^2)^2]/\Sigma \; [w(F_0^2)]\}^{1/2}$.

[b] Goodness of fit = $\{\Sigma \; w(F_0^2 - F_c^2)/N_{obs} - N_{parm})\}^{1/2}$.

TABLE 3
Atomic Coordinates (× 10^4), Equivalent Isotropic Displacement Parameters U_{eq} (Å^2 × 10^3) and Anisotropic Displacement Parameters U_{ij} (Å^2 × 10^3)

Atom	x	y	z	$U_{(eq)}$	U_{11}	U_{22}	U_{33}	U_{23}	U_{13}	U_{12}
W(1)	0	8584(1)[a]	2500	7(1)	8(1)	5(1)	7(1)	0	3(1)	0
W(2)	1268(1)	6487(1)	9638(1)	7(1)	9(1)	5(1)	5(1)	1(1)	4(1)	1(1)
Bi	2206(1)	3165(1)	8417(1)	14(1)	16(1)	13(1)	14(1)	5(1)	9(1)	5(1)
Te	4065(1)	3038(1)	8446(1)	9(1)	10(1)	9(1)	7(1)	−3(1)	5(1)	−2(1)
O(1)	467(5)	6538(15)	3771(7)	13(2)	13(4)	13(4)	7(3)	−4(3)	2(3)	−1(3)
O(2)	3066(5)	3918(18)	7798(8)	16(2)	13(4)	25(5)	19(4)	6(4)	13(3)	3(4)
O(3)	420(4)	8444(15)	8759(7)	12(2)	7(3)	12(4)	11(3)	−2(3)	2(3)	−1(3)
O(4)	1958(4)	8731(14)	0267(7)	10(2)	8(3)	8(4)	8(3)	0(3)	0(3)	−3(3)
O(5)	1184(4)	6063(14)	7935(7)	9(1)	14(3)	8(4)	2(3)	1(3)	3(3)	−1(3)
O(6)	867(4)	9158(14)	2415(7)	10(1)	14(4)	6(3)	12(3)	2(3)	9(3)	5(3)
O(7)	1248(5)	5700(15)	0967(7)	11(2)	18(4)	10(4)	9(3)	−2(3)	9(3)	−6(3)
O(8)	1958(5)	3878(15)	9921(7)	11(2)	14(4)	10(4)	8(3)	2(3)	6(3)	5(3)

Note. $U_{(eq)} = \frac{1}{3}(U_{11}a^{*2}a^2 + U_{22}b^{*2}b^2 + U_{33}c^{*2}c^2 + U_{12}a^*b^*ab\cos\gamma + U_{13}a^*c^*ac\cos\beta + U_{23}b^*c^*bc\cos\alpha)$; the anisotropic displacement exponent takes the form $-2\pi^2[h^2a^{*2}U_{11} + \cdots + 2\,hka^*b^*U_{12}]$.
[a] e.s.d.'s are in parentheses.

TABLE 4
Main Interatomic Distances (Å), Angles (°), and Bond Valences in $Bi_2Te_2W_3O_{16}$

BiO_8 square antiprism, ⟨Bi–O⟩ = 2.484 Å

Bi	O(8)1	O(8)2	O(4)1	O(2)	O(5)1	O(7)2	O(6)	O(2)1	V_{ij}
O(8)1	**2.182(8)**[b]	2.689(18)	2.901(12)	3.343(13)	4.313(13)	4.799(13)	3.925(12)	3.305(14)	0.78
O(8)2	73.4(3)	**2.304(7)**	2.788(12)	4.494(14)	2.444(13)	4.417(13)	3.197(12)	4.429(13)	0.56
O(4)1	73.1(3)	78.9(3)	**2.376(8)**	2.832(13)	3.277(12)	4.300(13)	4.895(12)	4.925(13)	0.46
O(2)	145.1(3)	93.3(3)	72.7(3)	**2.407(8)**	4.274(13)	3.221(14)	4.744(13)	3.474(20)	0.42
O(5)1	61.3(3)	134.5(3)	84.6(3)	121.6(3)	**2.492(8)**	2.782(13)	2.976(12)	4.575(13)	0.33
O(7)2	124.0(2)	158.9(3)	115.8(3)	78.0(3)	64.8(2)	**2.694(8)**	3.085(12)	3.324(14)	0.19
O(6)	78.8(3)	106.3(3)	148.7(3)	136.0(3)	69.7(3)	69.6(2)	**2.710(8)**	2.660(13)	0.19
O(2)1	84.4(3)	123.9(3)	151.4(3)	85.4(2)	123.2(3)	75.8(3)	58.8(2)	**2.711(9)**	0.19
$\sum V_{ij}$									**3.12**

$W(1)O_6$ octahedron, ⟨W(1)–O⟩ = 1.944 Å

W(1)	O(1)	O(1)1	O(6)	O(6)1	O(3)	O(3)1	V_{ij}
O(1)	**1.769(8)**	2.704(18)	2.767(12)	2.744(12)	2.795(13)	3.865(13)	1.51
O(1)1	99.9(5)	**1.769(8)**	2.744(12)	2.767(12)	3.865(13)	2.795(13)	1.51
O(6)	95.6(4)	96.6(4)	**1.935(8)**	2.817(7)	2.635(12)	2.737(12)	0.96
O(6)1	96.6(4)	95.6(4)	160.9(5)	**1.935(8)**	2.737(12)	2.635(12)	0.96
O(3)	91.2(3)	168.7(3)	84.6(3)	80.6(3)	**2.129(8)**	2.675(18)	0.57
O(3)1	168.7(3)	91.2(3)	80.6(3)	84.6(3)	77.9(4)	**2.129(8)**	0.57
$\sum V_{ij}$							**6.08**

$W(2)O_6$ octahedron, ⟨W(2)–O⟩ = 1.940 Å

W(2)	O(4)	O(7)	O(3)	O(8)	O(5)	O(1)2	V_{ij}
O(4)	**1.745(8)**	2.738(13)	2.718(12)	2.739(13)	2.890(12)	3.948(13)	1.61
O(7)	101.4(4)	**1.785(7)**	2.805(13)	2.718(13)	3.823(13)	2.647(13)	1.44
O(3)	98.1(4)	101.0(4)	**1.853(8)**	3.730(13)	2.729(12)	2.778(13)	1.20
O(8)	95.6(3)	93.3(4)	157.9(3)	**1.950(8)**	2.444(13)	2.656(13)	0.92
O(5)	96.9(3)	158.7(3)	86.9(3)	74.2(3)	**2.104(7)**	2.726(13)	0.61
O(1)2	173.7(3)	82.5(3)	85.9(3)	79.2(3)	78.4(3)	**2.204(8)**	0.46
$\sum V_{ij}$							**6.24**

TeO_4 disphenoid, $\langle Te–O\rangle_{moy.}$ = 2.037 Å

Te	O(2)	O(5)	O(6)	O(7)	V_{ij}
O(2)	**1.863(8)**	2.767(13)	2.660(13)	2.948(14)	1.36
O(5)	94.8(4)	**1.891(7)**	2.735(12)	2.782(13)	1.26
O(6)	88.0(4)	90.3(3)	**1.965(8)**	4.368(13)	1.03
O(7)	85.5(4)	79.1(3)	167.1(3)	**2.431(8)**	0.29
$\sum V_{ij}$					**3.94**

[a] Notations are those indicated in Figs. 2–4.
[b] e.s.d.'s are given in parentheses.

TABLE 5
Bond Lengths (Å) and Bond Valences in OM_{2-4} Polyhedra

	Bond length	V_{ij}		Bond length	V_{ij}
O(1)–W(1)	1.769	1.51	O(5)–W(2)	2.104	0.61
O(1)–W(2)	2.204	0.46	O(5)–Te	1.891	1.26
O(1)–Te	3.241	0.03	O(5)–Bi	2.492	0.33
O(1)–Te	3.772	0.01	O(5)–W(1)	3.439	0.02
ΣV_{ij}		2.01	ΣV_{ij}		2.22
O(2)–Te	1.863	1.36	O(6)–W(1)	1.935	0.96
O(2)–Bi	2.407	0.42	O(6)–Te	1.965	1.03
O(2)–Bi	2.711	0.19	O(6)–Bi	2.710	0.19
O(2)–W(2)	3.769	0.01	O(6)–W(2)	3.471	0.01
ΣV_{ij}		1.98	ΣV_{ij}		2.19
O(3)–W(2)	1.853	1.20	O(7)–W(1)	1.785	1.44
O(3)–W(1)	2.129	0.57	O(7)–Te	2.431	0.29
O(3)–Te	2.692	0.15	O(7)–Bi	2.694	0.19
O(3)–Te	3.684	0.01	O(7)–Bi	3.638	0.02
ΣV_{ij}		1.93	ΣV_{ij}		1.94
O(4)–W(2)	1.745	1.61	O(8)–W(2)	1.950	0.92
O(4)–Bi	2.376	0.46	O(8)–Bi	2.182	0.78
ΣV_{ij}		2.07	O(3)–Bi	2.304	0.56
			ΣV_{ij}		2.26

for W(1), 0.56 Å for W(2)], and already observed in the $Bi_2Te_2WO_{10}$ crystal structure (7), simply corresponds to the strengthening of the bonds of the corresponding tungsten atom with the oxygen atoms which are only weakly bonded to other cations (see Table 5 and Fig. 2).

The bismuth atoms are surrounded by eight oxygen atoms at distances ranging from 2.18 to 2.71 Å. The corresponding polyhedron is the distorted square antiprism

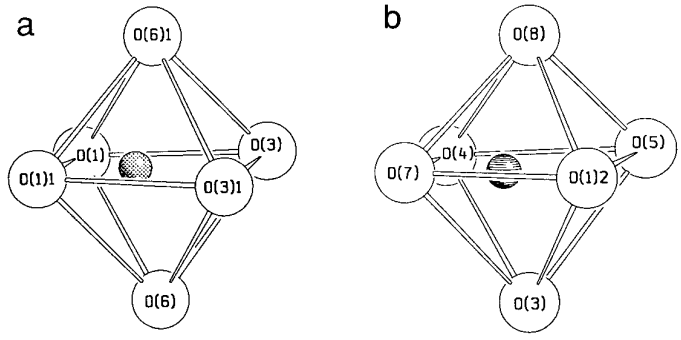

FIG. 2. Spatial views of the W coordination polyhedra: (a) $W(1)O_6$ octahedron, (b) $W(2)O_6$ octahedron.

shown in Fig. 3. The mean distance $\langle Bi–O \rangle = 2.48$ Å is not very different from the sum of ionic radii (2.52–2.53 Å). The disparity of the distances, however, reveals the weak stereochemical activity of the lone pair E of bismuth atoms, probably directed toward the center of the O(2)1–O(6)–O(7)2 face.

As for the tellurium atoms, for which the lone pair is strongly active, their coordination polyhedron can be described in one of two ways:

1. As a slightly distorted TeO_3 triangular pyramid whose more strongly bonded three oxygen atoms O(2), O(5), and O(6) constitute the base and Te the apex, with the lone pair E so directed as to constitute the fourth vertex of a TeO_3E tetrahedron (Fig. 4a). The TeO_3 pyramid is a commonly accepted feature of the crystal chemistry of tellurium(IV) compounds.
2. As a highly distorted trigonal bipyramid TeO_4E if we

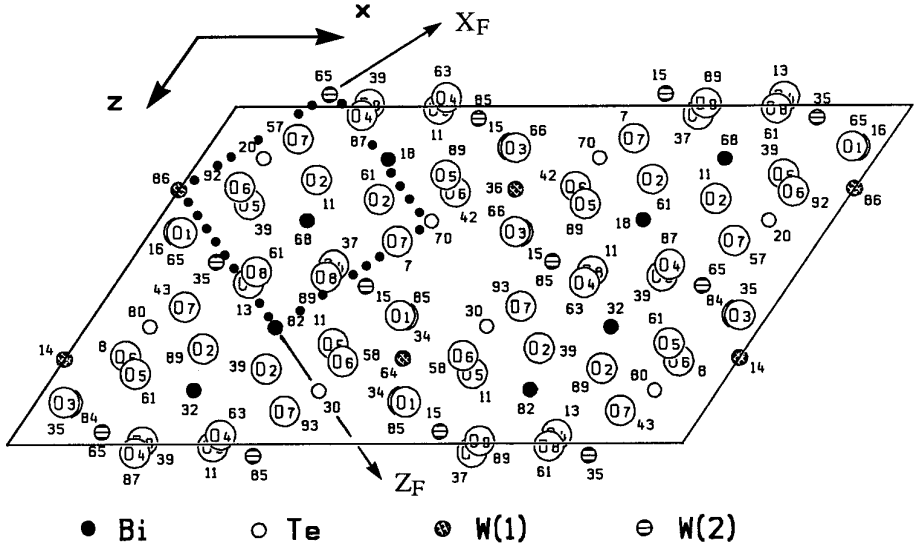

FIG. 1. Projection of the $Bi_2Te_2W_3O_{16}$ crystal structure onto (010).

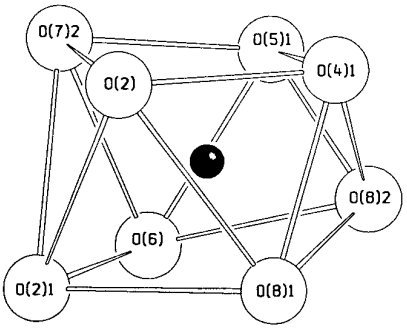

FIG. 3. Distorted BiO_8 square antiprism.

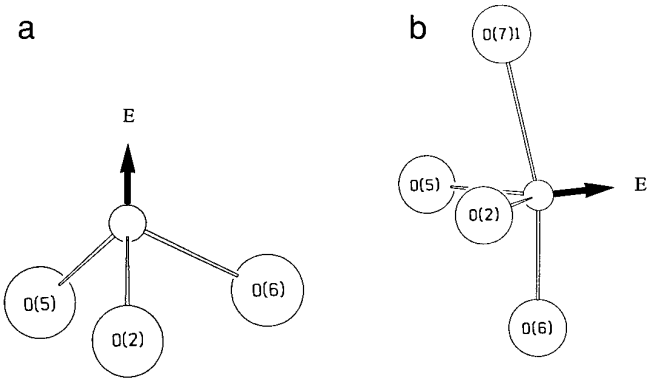

FIG. 4. Perspective views of the Te(IV) coordination polyhedra: (a) TeO_3 pyramid, (b) TeO_4 disphenoid [the arrows visualize the direction toward which the lone pair E of Te(IV) atoms is stereochemically active].

take into account the bonded O(7)1 atom (Fig. 4b). The TeO_4 disphenoid is also frequently observed in Te(IV) mixed oxides.

Each BiO_8 square antiprism shares its O(8)–O(8) edge with another square antiprism to form a Bi_2O_{14} unit. As shown in Fig. 5 each Bi_2O_{14} unit shares the following:

—four O(2) corners with four identical Bi_2O_{14} units,
—two O(5)–O(8) edges with two different $W(2)O_6$ octahedra,
—the O(4) and O(7) corners with four $W(2)O_6$ octahedra, and
—two O(2)–O(6) and two O(5)–O(7) edges with four TeO_4 disphenoids.

The $[Bi_2Te_2W(2)_2O_{16}]$ complex layers so constituted, parallel to (100), are connected via $W(1)O_6$ octahedra by sharing O(1) and O(3) corners. The corresponding three-dimensional polyhedral network is represented in Fig. 6. We can clearly see that it contains large pseudohexagonal tunnels, parallel to Oy, toward the center of which are roughly directed the lone pairs E of tellurium atoms.

RELATIONSHIPS WITH THE FLUORITE STRUCTURE AND THE FLUORITE-RELATED $Bi_7F_5O_{11}$ STRUCTURE

As shown by the projection in Fig. 1 the cations are distributed at the corners of a distorted face-centered cubic network ($a_F \approx 5.65$ Å) with distances between nearest neighbors ranging from 3.42 to 5.05 Å. A large portion of

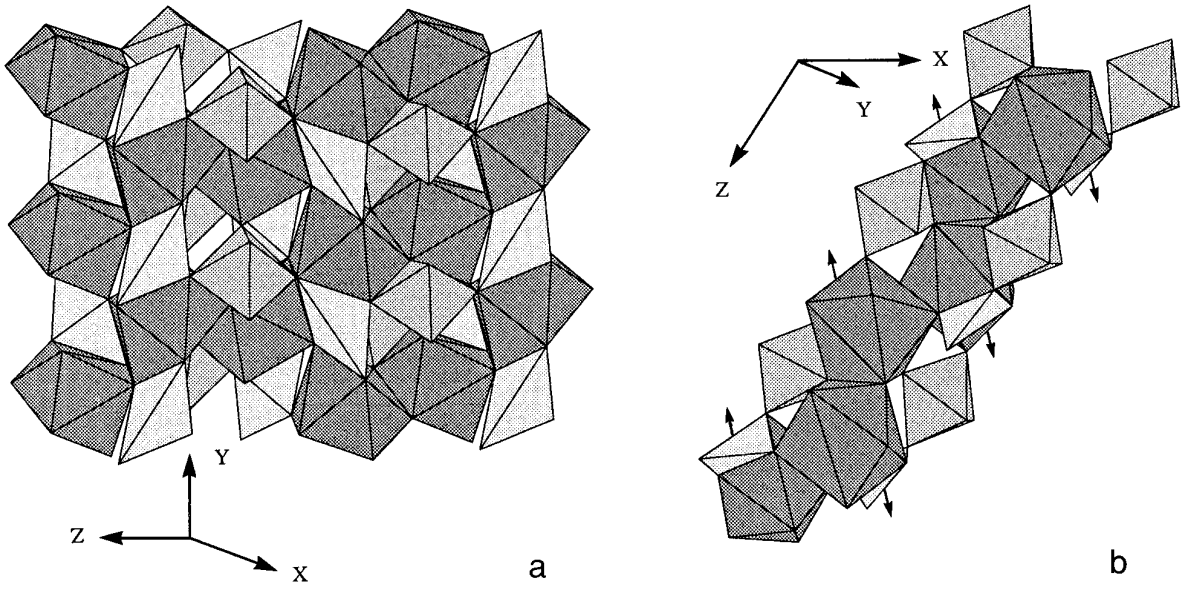

FIG. 5. $[Bi_2Te_2W_2O_{16}]$ complex layer in the $Bi_2Te_2W_3O_{16}$ crystal structure: (a) perspective view parallel to (100), (b) perspective view along [010].

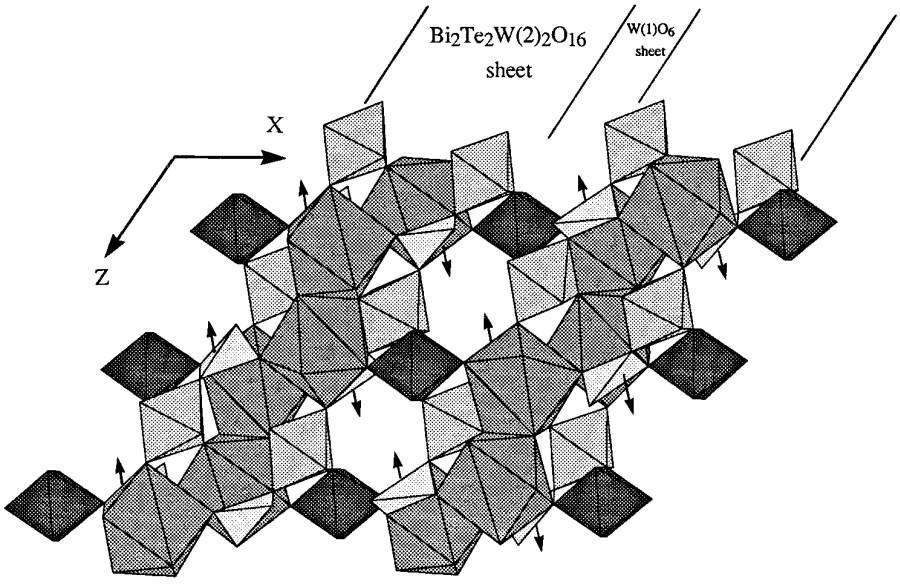

FIG. 6. Three-dimensional polyhedral network $Bi_2Te_2W_3O_{16}$.

the anions [O(1), O(2), O(3), O(5), O(6), and O(7)] are approximately located in the tetrahedral sites of this network and correspond to "normal" anions of the parent fluorite structure. The other anions [O(4) and O(8)] are grouped together in densified areas (shaded parts of Fig. 7a) corresponding to infinite columns of $Bi_2W(2)_2$ tetrahedra. $Bi_2Te_2W_3O_{16}$ can therefore be considered as an anion-excess, cation-ordered, fluorite-related superstructure. The relationships of the corresponding supercell (subscript S) to the fluorite subcell (subscript F) are

$$\begin{vmatrix} a_S \\ b_S \\ c_S \end{vmatrix} = \begin{vmatrix} 3 & 0 & 2 \\ 0 & 1 & 0 \\ \bar{2} & 0 & 1 \end{vmatrix} \begin{vmatrix} a_F \\ b_F \\ c_F \end{vmatrix}.$$

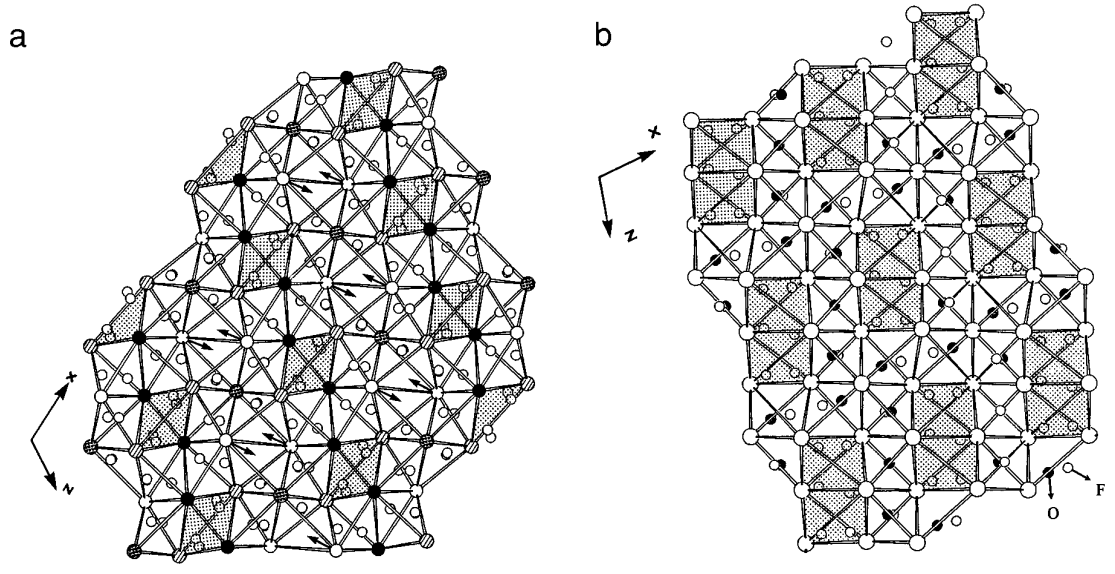

FIG. 7. [010] projection visualizing how the anionic densification results from a regular insertion of zig-zag [010] rows of anions within the cationic tetrahedral network in (a) the $Bi_7F_{11}O_5$ structure and (b) the $Bi_2Te_2W_3O_{16}$ structure (cations are differentiated in the same way as in Fig. 1). (The densified areas are shaded.)

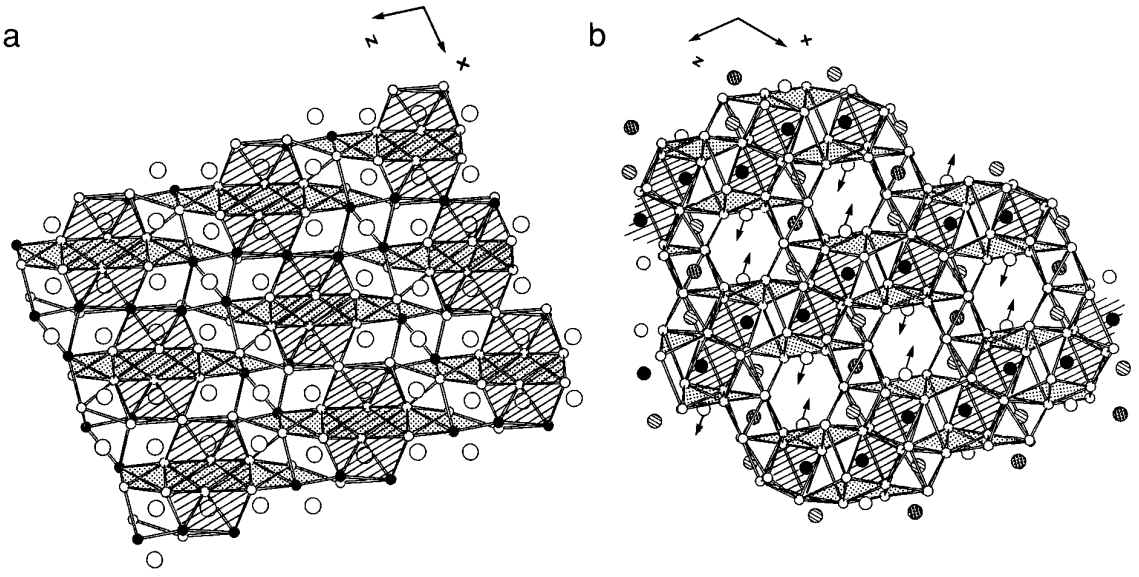

FIG. 8. Representation of the $Bi_7F_{11}O_5$ (a) and $Bi_2Te_2W_3O_{16}$ (b) structures as fluorite-related superstructures with columnar clusters. (The densified and corrugated parts of the anionic subcell are shaded; the clusters are hatched.)

The change from the fluorite parent structure (MX_2) to the $Bi_2Te_2W_3O_{16}$ (M_7X_{16}) structure is obvious: it simply results from an ordered insertion, every seventh XM_4 tetrahedron, of an extra anionic row, parallel to $[010]_F$ [here an extra O(4)–O(8) row]. This structural change can be formulated as:

$$7XM_{4/8} + X \rightarrow M_{7/2}X_8(M_7X_{16})$$

or, more precisely,

$$7O\,[Bi_{2/14}Te_{2/14}W_{3/14}] + O \rightarrow BiTeW_{3/2}O_8\,(Bi_2Te_2W_3O_{16}).$$

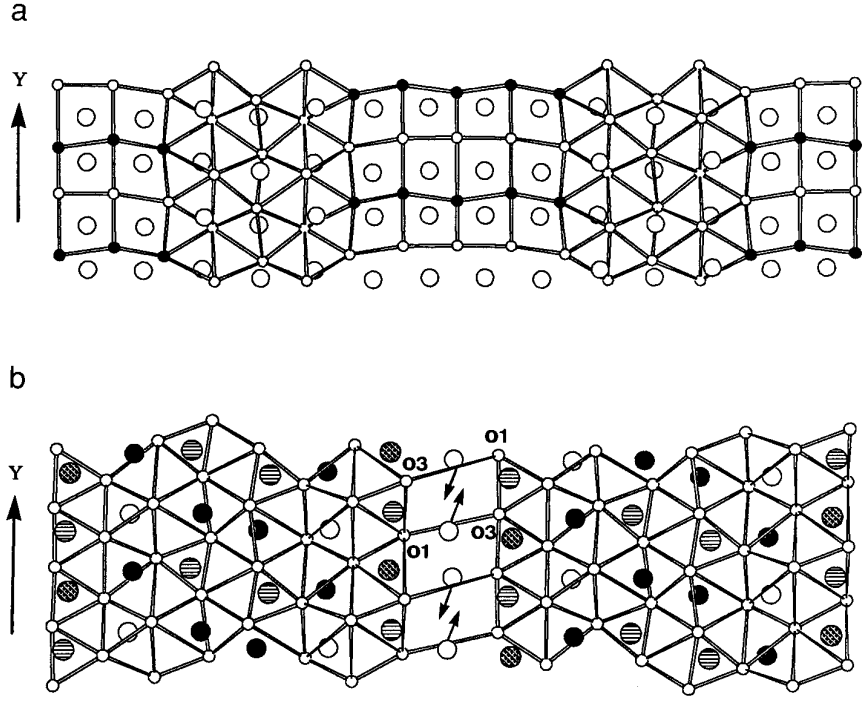

FIG. 9. Projections along the direction perpendicular to the densified anionic layers of (a) the $Bi_7F_{11}O_5$ structure and (b) the $Bi_2Te_2W_3O_{16}$ structure.

Such densification is only possible thanks to the strong distortion of both the cationic and anionic subcells resulting in a great change in cation-to-anion coordination: the MO_8 anionic cubes characteristic of the fluorite structure are either strongly distorted or replaced by other polyhedra. As a consequence the tetrahedral coordination of anions is no longer preserved; the oxygen atoms are set off-center toward a triangular face or an edge and are therefore in threefold or twofold coordination (see Table 5). In fact, these distortions are the consequences of both the anionic insertion and the stereochemical activity of tellurium lone pairs E. One can clearly see in Figs. 1 and 7a how the extra anions O(4) and O(8), on the one hand, and the stereochemically active lone pairs E, on the other hand, push away respectively the O(2), O(7) anions and W(2) cations [W(2)–W(2) = 4.92 Å] and the O(1), O(3) anions and Te cations (Te–Te = 5.05 Å).

We have recently solved the crystal superstructure of another M_7X_{16} ordered anion-excess, fluorite-related compound $Bi_7F_{11}O_5$ (8). We have shown that it can also be described as the member $m' = 7$ (or $m = 5$) of the $M_{m'}X_{2m'+2}$ (or $M_{m+2}X_{2m+4}$) series of fluorite-related superstructures with infinite columnar clusters (9) and as the member $n = 3.5$ of a M_nX_{2n+1} series of new Vernier phases, which we called the ''shifted Vernier phases'' (10).

In these new Vernier structures the clusters (or densified areas) are no longer aligned and directly connected along rows perpendicular to the densified anionic layers; they are now shifted, from one densified plane to the other, by the vector $\boldsymbol{\tau} = p(\mathbf{a}_F + \mathbf{b}_F)/2$ ($p = 1$ for $Bi_7F_{11}O_5$) parallel to the densified layers (see Fig. 8a).

Comparison of Figs. 7a and 7b reveals the strong analogies that exist between the two M_7X_{16} superstructures: both derive from the parent fluorite structure by the same periodic insertion of an extra row of anions parallel to one $\langle 100\rangle_F$ direction. Large differences, however, have to be pointed out:

1. Because of the presence of only one kind of cation, a large mean size of the fluorite subcell ($a_F \approx 5.79$ Å against 5.65 Å for $Bi_2Te_2W_3O_{16}$), and a strictly ordered distribution of two different anions O^{2-} and F^-, the cationic and anionic fluorite subcells are much less distorted in the $Bi_7F_{11}O_5$ structure than in the $Bi_2Te_2W_3O_{16}$ structure.

2. If both structures can be considered as members $m' = 7$ of the $M_{m'}X_{2m'+2}$ series of fluorite-related superstructures with columnar clusters, the nature of these clusters is quite different. In $Bi_7F_{11}O_5$, they correspond to infinite *cis*-chains of corner-sharing BiF_6O_2 polyhedra (distorted square antiprisms or bicapped trigonal prisms: densified YF_3-like part of the structure) (Fig. 8a). In $Bi_2Te_2W_3O_{16}$ they are constituted by an infinite column, parallel to Oy, of pairs Bi_2O_{14} of BiO_8 square antiprisms sharing, at the same level, a O(8)–O(8) edge, and connected along Oy via the $W(2)O_6$ octahedra (Figs. 6 and 8b).

3. As shown by the comparison of the two $\langle 100\rangle_F$-type projections realized along the direction perpendicular to the densified anionic layers (Fig. 9), only the $Bi_7F_{11}O_5$ structure can really be described in terms of a family II Vernier structure, i.e., a structure in which densified 3^6 hexagonal strips of the anionic layers alternate with unmodified 4^4 fluorite-like strips (Fig. 9a). In the case of the $Bi_2Te_2W_3O_{16}$ structure, the stereochemically very active lone pairs of Te atoms create a second ''artificial densification'' of the $\langle 100\rangle_F$ anionic layers, pushing away the O(1) and O(3) anions and then distorting what could have been, with a ''normal cation,'' the 4^4 fluorite-like strips.

REFERENCES

1. A. Chagraoui, P. Marchet, P. Thomas, and J. C. Champarnaud-Mesjard, Vth European Conference on Solid State Chemistry, Montpellier, France, Sept. 4–7, Vol. B39, p. 312 (1995).
2. J. W. Wisser, *J. Appl. Crystallogr.* **2,** 89 (1969).
3. G. M. Sheldrick, ''SHELXTL PC, Version 4.1: An Integrated System for Solving, Refining and Displaying Crystal Structures from Diffraction Data.'' Siemens Analytical X-ray Instruments, Inc., Madison, WI, 1988.
4. G. M. Sheldrick, ''SHELXL-93: Program for Refinement of Crystal Structures.'' University of Göttingen, 1993.
5. N. E. Brese and M. O'Keeffe, *Acta Crystallogr. B* **47,** 192 (1991).
6. R. D. Shannon, *Acta Crystallogr. A* **32,** 751 (1976).
7. J. C. Champarnaud-Mesjard, B. Frit, A. Chagraoui, and A. Tairi, *Z. Anorg. Allg. Chem.* **662,** 1907 (1996).
8. J. P. Laval, J. C. Champarnaud-Mesjard, B. Frit, A. Britel, and A. Mikou, *Eur. J. Solid State Inorg. Chem.* **21,** 943 (1994).
9. B. Frit and J. P. Laval, *J. Solid State Chem.* **39,** 85 (1981).
10. B. Frit, J. P. Laval, and J. Strähle, *Aust. J. Chem.* **49,** 883 (1996).